Video Article

Synthesis Method for Cellulose Nanofiber Biotemplated Palladium Composite Aerogels

Fred J. Burpo[1], Jesse L. Palmer[1], Alexander N. Mitropoulos[1,2], Enoch A. Nagelli[1], Lauren A. Morris[3], Madeline Y. Ryu[1], John Wickiser[1]

[1]Department of Chemistry and Life Science, United States Military Academy

[2]Department of Mathematical Sciences, United States Military Academy

[3]Armament Research, Development and Engineering Center, U.S. Army RDECOM-ARDEC

Correspondence to: Fred J. Burpo at john.burpo@westpoint.edu

URL: https://www.jove.com/video/59176
DOI: doi:10.3791/59176

Keywords: cellulose, aerogel, hydrogel, porous, composites, palladium, noble metal

Date Published: 12/13/2018

Citation: Burpo, F.J., Palmer, J.L., Mitropoulos, A.N., Nagelli, E.A., Morris, L.A., Ryu, M.Y., Wickiser, J. Synthesis Method for Cellulose Nanofiber Biotemplated Palladium Composite Aerogels. *J. Vis. Exp.* (), e59176, doi:10.3791/59176 (2018).

Abstract

Here, a method to synthesize cellulose nanofiber biotemplated palladium composite aerogels is presented. Noble metal aerogel synthesis methods often result in fragile aerogels with poor shape control. The use of carboxymethylated cellulose nanofibers (CNFs) to form a covalently bonded hydrogel allows for the reduction of metal ions such as palladium on the CNFs with control over both nanostructure and macroscopic aerogel monolith shape after supercritical drying. Crosslinking the carboxymethylated cellulose nanofibers is achieved using 1-ethyl-3-(3-dimethylaminopropyl) carbodiimide hydrochloride (EDC) in the presence of ethylendiamine. The CNF hydrogels maintain their shape throughout synthesis steps including covalent crosslinking, equilibration with precursor ions, metal reduction with high concentration reducing agent, rinsing in water, ethanol solvent exchange, and CO_2 supercritical drying. Varying the precursor palladium ion concentration allows for control over the metal content in the final aerogel composite through a direct ion chemical reduction rather than relying on the relatively slow coalescence of pre-formed nanoparticles used in other sol-gel techniques. With diffusion as the basis to introduce and remove chemical species into and out of the hydrogel, this method is suitable for smaller bulk geometries and thin films. Characterization of the cellulose nanofiber-palladium composite aerogels with scanning electron microscopy, X-ray diffractometry, thermal gravimetric analysis, nitrogen gas adsorption, electrochemical impedance spectroscopy, and cyclic voltammetry indicates a high surface area, metallized palladium porous structure.

Introduction

Aerogels, first reported by Kistler, offer porous structures orders of magnitude less dense than their bulk material counterparts[1,2,3]. Noble metal aerogels have attracted scientific interest for their potential in power and energy, catalytic, and sensor applications. Noble metal aerogels have recently been synthesized via two basic strategies. One strategy is to induce the coalescence of pre-formed nanoparticles[4,5,6,7]. Sol-gel coalescence of nanoparticles can be driven by linker molecules, changes in solution ionic strength, or simple nanoparticle surface free energy minimization[7,8,9]. The other strategy is to form aerogels in a single reduction step from metal precursor solutions[9,10,11,12,13]. This approach has also been used to form bimetallic and alloy noble metal aerogels. The first strategy is generally slow and may require up to many weeks for nanoparticle coalescence[14]. The direct reduction approach, while generally more rapid, suffers from poor shape control over the macroscopic aerogel monolith.

One possible synthesis approach to address challenges with control of noble metal aerogel macroscopic shape and nanostructure is to employ biotemplating[15]. Biotemplating uses biological molecules ranging from collagen, gelatin, DNA, viruses, to cellulose to provide a shape-directing template for the synthesis of nanostructures, where the resulting metal-based nanostructures assume the geometry of the biological template molecule[16,17]. Cellulose nanofibers are appealing as a biotemplate given the high natural abundance of cellulosic materials, their high aspect ratio linear geometry, and ability to chemically functionalize their glucose monomers[18,19,20,21,22,23]. Cellulose nanofibers (CNF) have been used to synthesize three dimensional TiO_2 nanowires for photoanodes[24], silver nanowires for transparent paper electronics[25], and palladium aerogel composites for catalysis[26]. Further, TEMPO-oxidized cellulose nanofibers have been used both as a biotemplate and reducing agent in the preparation of palladium decorated CNF aerogels[27].

Here, a method to synthesize cellulose nanofiber biotemplated palladium composite aerogels is presented[26]. Fragile aerogels with poor shape control occurs for a range noble metal aerogel synthesis methods. Carboxymethylated cellulose nanofibers (CNFs) used to form a covalent hydrogel allow for the reduction of metal ions such as palladium on the CNFs providing control over both nanostructure and macroscopic aerogel monolith shape after supercritical drying. Carboxymethylated cellulose nanofiber crosslinking is achieved using 1-ethyl-3-(3-dimethylaminopropyl) carbodiimide hydrochloride (EDC) in the presence of ethylendiamine as a linker molecule between CNFs. The CNF hydrogels maintain their shape throughout the synthesis steps including covalent crosslinking, equilibration with precursor ions, metal reduction with high concentration reducing agent, rinsing in water, ethanol solvent exchange, and CO_2 supercritical drying. Precursor ion concentration variation allows for control over the final aerogel metal content through a direct ion reduction rather than relying on the relatively slow coalescence of pre-formed nanoparticles used in sol-gel methods. With diffusion as the basis to introduce and remove chemical species into and out of the hydrogel, this method is suitable for smaller bulk geometries and thin films. Characterization of the cellulose nanofiber-

palladium composite aerogels with scanning electron microscopy, X-ray diffractometry, thermal gravimetric analysis, nitrogen gas adsorption, electrochemical impedance spectroscopy, and cyclic voltammetry indicates a high surface area, metalized palladium porous structure.

Protocol

CAUTION: Consult all relevant safety data sheets (SDS) before use. Use appropriate safety practices when performing chemical reactions, to include the use of a fume hood and personal protective equipment (PPE). Rapid hydrogen gas evolution can cause high pressure in reaction tubes causing caps to pop and solutions to spray out. Ensure that reaction tubes remain open and pointed away from the experimenter as specified in the protocol.

1. Cellulose nanofiber hydrogel preparation

1. Preparation of cellulose nanofiber solution: Prepare 3% (w/w) cellulose nanofiber solution by mixing 1.5 g of carboxymethyl cellulose nanofibers with 50 mL of deionized water. Shake the solution and vortex for 1 min. Sonicate the solution in a bath sonicator at ambient temperature for 24 h to ensure complete mixing.
2. Preparation of cross-linking solution: First add 0.959 g of EDC and 0.195 g of 2-(N-morpholino)ethanesulfonic acid (MES) buffer to 2.833 mL of deionized water. Vortex. Add 0.167 mL of ethylenediamine. Vortex for 15 s. Adjust the final volume to 10 mL and pH to 4.5 by adding 1.0 M HCl and deionized water.
   NOTE: Final crosslinking solution concentrations are 0.5 M EDC, 0.25 M ethylenediamine, and 0.1 M MES buffer.
3. Centrifugation of cellulose nanofiber solution: Pipette 0.25 mL of the 3 % (w/w) cellulose nanofiber solution into each of 6 microfuge tubes (1.7 mL or 2.0 mL). Centrifuge the microfuge tubes for 20 min at 21,000 x g. Remove excess water above the compacted CNFs with a pipette avoiding contact with the top surface.
   NOTE: After centrifuging, the cellulose nanofiber solutions present a distinct interface between the concentrated CNF's and the clear supernatant. Based on removal of the excess water, the final CNF concentration will be approximately 3.8%.
4. Cross-link the cellulose nanofiber hydrogels. Pipette 1.0 mL of the EDC and diamine crosslinking solution above the compacted cellulose nanofibers in each of the microfuge tubes. Wait at least 24 h for the crosslinking solution to diffuse through the gels and crosslink the CNFs.
5. Gel rinsing: Remove the crosslinking solution supernatant in the microfuge tubes with a pipette. With the microfuge tube caps open, immerse the microfuge tubes containing the crosslinked CNF gels in 1 L of deionized water for at least 24 h to remove excess crosslinking solution from within the CNF hydrogels.
6. Fourier-transform infrared (FTIR) spectroscopy: Place approximately 0.5 mL of 3% (w/w) CNF solution in deionized water on the sample stage and scan percent transmittance for 650 - 4000 cm^{-1}. Use the same scan conditions and repeat for a CNF crosslinked hydrogel from Step 1.5.

2. Preparation of cellulose nanofiber - palladium composite hydrogels

1. Prepare $Pd(NH_3)_4Cl_2$ solution. Prepare 10 mL of 1.0 M $Pd(NH_3)Cl_2$ solution. Vortex the solution for 15 s. Dilute 1.0 M $Pd(NH_3)Cl_2$ solution to 1 mL volumes at 1, 10, 50, 100, 500, and 1000 mM.
   NOTE: 1.0 M $NaPdCl_4$ solution and respective dilutions may be used and results in similar final aerogel structures.
2. Equilibrate cellulose nanofiber hydrogels in palladium solutions. Pipette 1 mL of the 1, 10, 50, 100, 500, and 1000 mM $Pd(NH_3)Cl_2$ solutions on the top of the cellulose nanofiber hydrogels in the microfuge tubes. Wait at least 24 h for the palladium solution to equilibrate within the hydrogels.
3. Prepare $NaBH_4$ reducing agent solution. Prepare 60 mL of 2 M $NaBH_4$ solution. Aliquot 10 mL of $NaBH_4$ solution into each of six 15 mL conical tubes.
   NOTE: The 2 M $NaBH_4$ solution is a highly concentrated reducing agent solution and should be handled within a chemical fume hood. Spontaneous decomposition and hydrogen gas evolution will be observed. Ensure that the tubes are pointed away from the experimenter and that proper PPE is worn.
4. First reduction of palladium salts on cellulose nanofiber hydrogels: Invert the microfuge tubes with the palladium equilibrated CNF hydrogels and gently tap to remove the hydrogels. In a chemical fume hood, with flat tweezers, place each of the palladium equilibrated CNF hydrogels into each of the 15 mL conical tubes with 10 mL of $NaBH_4$ solution. Allow the reduction to proceed for 24 h.
   NOTE: Upon placing the palladium equilibrated CNF gels into the 2 M $NaBH_4$ solution, violent hydrogen gas evolution will occur. Ensure that reaction tubes remain open and pointed away from the experimenter.
5. Prepare second $NaBH_4$ reducing agent solution. Prepare 60 mL of 0.5 M $NaBH_4$ solution. Aliquot 10 mL of $NaBH_4$ solution into each of six 15 mL conical tubes.
6. Second reduction of palladium salts on cellulose nanofiber hydrogels: In a fume hood, using a pair of flat tweezers transfer each of hydrogels from the 2 M $NaBH_4$ solutions into the 0.5 M $NaBH_4$ solutions. Allow the reduction to proceed for 24 h.
   NOTE: The initially reduced CNF gels in the 2 M $NaBH_4$ solution will be mechanically stable during the transfer step. However, light pressure should be used with the flat tweezers during solution transfer steps to avoid gel compaction.
7. Rinse the cellulose nanofiber-palladium composite gels. Using flat tweezers, transfer each of the reduced palladium-CNF gels into 50 mL deionized water in conical tubes. Exchange deionized water after 12 h and allow the gels to rinse for at least an additional 12 h.
8. Perform ethanol solvent exchange in cellulose nanofiber-palladium gels. Use flat tweezers to transfer the rinsed CNF-palladium gels successively into 50 mL of 25%, 50%, 75%, and 100% ethanol solutions with at least 6 h in each solution.

3. Aerogel preparation

1. After solvent exchange with ethanol, dry the CNF-palladium gels using CO_2 in a supercritical dryer with a set point of 35 °C and 1200 psi. After supercritical drying is complete, allow the chamber to equilibrate for at least 12 h prior to opening and removal of the aerogels.

NOTE: Occasionally, the 500 mM and 1000 mM samples have been observed to combust when removed from the supercritical dryer which is attributed to the presence of palladium hydride. The 12 h supercritical chamber equilibration is intended to allow for outgassing of hydrogen.

4. Composite aerogel material characterization

1. Scanning electron microscopy (SEM): Cut the CNF-palladium aerogel with a razor blade to obtain a thin film approximately 1 - 2 mm thick. Affix the thin film sample with carbon tape on a SEM sample stub. Initially use an accelerating voltage of 15 kV and beam current of 2.7 - 5.4 pA to perform imaging.
2. X-ray diffractometry (XRD): Place the CNF-palladium aerogel in a sample holder and align the top of the aerogel with the top of holder. Alternatively, place a thin film sample section, as in Step 4.1, on a glass slide. Perform XRD scans for diffraction angles 2Θ from 5 ° to 90 ° at 45 kV and 40 mA with Cu K_α radiation (1.54060 Å), a 2 θ step size of 0.0130 °, and 20 s per step.
3. Thermal gravimetric analysis (TGA): Place the aerogel sample in the instrument crucible. Perform analysis by flowing nitrogen gas at 60 mL/min and heating at 10 °/min from ambient temperature to 700 °C.
4. Nitrogen gas adsorption-desorption: Degas the samples for 24 h at room temperature. Use nitrogen at -196 °C as the test gas with equilibration times for adsorption and desorption of 60 s and 120 s, respectively.
   NOTE: Elevated degas temperatures are not recommended to avoid decomposition of the cellulose nanofibers.
5. **Electrochemical characterization.**
   1. Immerse the aerogel samples in 0.5 M H_2SO_4 electrolyte for 24 h.
   2. Use a 3-electrode cell with a Ag/AgCl (3 M NaCl) reference electrode, a 0.5 mm diameter Pt wire auxiliary/counter electrode, and a lacquer coated 0.5 mm diameter platinum working electrode. Place the lacquer coated wire with a 1 mm exposed tip in contact with the top surface of the aerogel at the bottom of the electrochemical vial[12].
   3. Perform electrochemical impedance spectroscopy (EIS) from 1 MHz to 1 mHz with a 10 mV sine wave.
   4. Perform cyclic voltammetry (CV) using a voltage range of −0.2 to 1.2 V (vs. Ag/AgCl) with scan rates of 10, 25, 50, 75, and 100 mV/s.

Representative Results

The scheme to covalently crosslink cellulose nanofibers with EDC in the presence of ethylendiamine is depicted in **Figure 1**. EDC crosslinking results in an amide bond between a carboxyl and primary amine functional group. Given that the carboxymethyl cellulose nanofibers possess only carboxyl groups for crosslinking, the presence of a diamine linker molecule such as ethylenediamine is essential to covalently link two adjacent CNFs via two amide bonds. To confirm crosslinking, **Figure 2** shows FTIR spectra for 3% (w/w) CNF solutions compared to CNF hydrogels after crosslinking with using EDC in the presence of ethylenediamine. Both CNF and crosslinked CNF hydrogels were equilibrated in deionized water prior to FTIR analysis. The 3% (w/w) CNF solution presents a broad peak between approximately 3200 to 3600 cm^{-1} and is attributed to O-H stretching[28]. The prominent peak at 1595 cm^{-1} is likely attributed to the vibration of the $-COO^-Na^+$ groups on the carboxymethyl cellulose nanofibers[29]. After crosslinking the carboxymethyl cellulose nanofibers with EDC in the presence of ethylenediamine, three bonding possibilities result. The first is an effective crosslink between two CNF's with ethylenediamine forming two amide bonds with carboxylates on the CNF's. The second is ethylenediamine forming a single amide bond with a CNF carboxylate with a primary amine at the other end of the diamine molecule. The third possibility is EDC forming an unstable o-acylisourea intermediate that hydrolyzes to reform the initial carboxyl group[30].

After crosslinking, the broad O-H absorption band between 3200 to 3600 cm^{-1} decreases, with the emergence of prominent peaks at 3284 and 3335 cm^{-1}, attributed to primary amines and amide bonds resulting from both amides of crosslinked CNFs, and single amide bonds between CNFs and ethylenediamine resulting in a primary amine at the terminal end of the ethylenediamine molecule[28,31]. The peak at 2903 cm^{-1} associated with C-H stretching becomes more prominent after crosslinking and is attributed to the increased presence of $-NH_3^+$ from the terminal primary amines. The decrease in the carbonyl stretch at a wavenumber of 1595 cm^{-1} is attributed to the decreased number of $-COO^-Na^+$ groups due to crosslinking with ethylenediamine. The formation of amide bonds due to crosslinking is seen in the amide peaks at 1693 and 1668 cm^{-1}, as well as at 1540 cm^{-1}, and a small peak at 1236 cm^{-1} [28,29,31].

Figure 3 depicts photographs of each of the synthesis steps to include: the covalently crosslinked CNF hydrogels (**Figure 3a**); CNFs equilibrated across a concentration range of 1, 10, 50, 100, 500, and 1000 mM $Pd(NH_3)_4Cl_2$ (**Figure 3b**), or Na_2PdCl_4 (**Figure 3c**) solution; reduced CNF-palladium gels (**Figure 3d**); and supercritically dried aerogel composites (**Figure 3e**). The photographs demonstrate the shape control offered by this synthesis method.

The SEM images in **Figure 4a-f** depict composite CNF-palladium aerogels synthesized from 1, 10, 50, 100, 500, and 1000 mM $Pd(NH_3)_4Cl_2$ solutions, respectively. In general, the aerogels present interconnected fibrillary ligaments with increasing nanoparticle size correlating with increasing palladium solution concentration. The average nanoparticle diameters and pore sizes for lower concentration samples are: 1 mM) 12.6 ± 2.2 nm and 32.4 ± 13.3 nm; and 10 mM) 12.4 ± 2.0 nm and 32.2 ± 10.4 nm. Aerogels synthesized with 50 mM and higher palladium concentrations present more distinctly interconnected nanoparticles. The average nanoparticle diameters resulting from 50, 100, 500, and 1000 mM palladium synthesis concentrations are 19.5 ± 5.0 nm, 41.9 ± 10.0 nm, 45.6 ± 14.6 nm, and 59.0 ± 16.4 nm, respectively.

XRD spectra for 2 θ angles from 20 - 70 ° in **Figure 5** indicate peaks for palladium and palladium hydride indexed to Joint Committee on Powder Diffraction Standards (JCPDS) reference numbers 01-087-0643 and00-018-0951, respectively. The palladium hydride and palladium peaks become more convoluted with increasing palladium synthesis concentration, where they are not distinguishable at 1000 mM. The decrease in peak broadening correlates with the increase in nanoparticle diameters observed in **Figure 4**.

The thermogravimetric spectra shown in **Figure 6** indicate increasing metal content in the CNF-palladium composite aerogels with increasing synthesis palladium solution concentration. The weight% versus palladium synthesis concentration shown in **Figure 6c** demonstrates control of metal content in the aerogel composite between 0 - 75.5%.

Nitrogen adsorption-desorption isotherms, and corresponding cumulative pore volumes with differential pore volume are shown for aerogel composites synthesized from 1, 100, and 1000 mM palladium solutions in **Figure 7a-b**, **Figure 7c-d**, and **Figure 7e-f**, respectively. The physisorption data indicates type IV adsorption-desorption isotherms indicating mesoporous and macroporous structure. The Brunauer-Emmett-Teller (BET) specific surface areas were 582, 456, and 171 m^2/g for the 1, 100, and 1000 mM palladium samples, respectively, indicating decreasing specific surface area with increasing metal content[32]. Barrett-Joyner-Halenda (BJH) pore size analysis also indicates that as the aerogel palladium content increases, there is a decreasing frequency of mesopores[33]. Using BJH analysis of the desorption curves, the cumulative pore volumes (V_{pore}) for the 1, 100 and 1000 mM samples were 7.37 cm^3/g, 6.10 cm^3/g, and 2.40 cm^3/g. Average sample specific volumes (V_{sample}) were determined by measuring the volume and dividing by the sample mass. Aerogel porosities were 97.3%, 95.0%, and 90.4% for the 1, 100, and 1000 mM, respectively using Equation (1),

$$\% \text{ Porosity} = (V_{pore} / V_{sample}) \times 100 \% \quad (1)$$

With the same starting CNF covalent hydrogel and pore size distribution, sample porosities decrease with increasing metal content as the reduced metal fills the pore space.

Figure 8a shows the EIS spectra conducted in 0.5 M H_2SO_4 using a 10 mA amplitude sine wave across a frequency range of 140 kHz to 15 mHz. The incomplete semicircle in the high frequency region shown in **Figure 8b** indicates low charge transfer resistance and double layer capacitance for the CNF-palladium composite aerogel. CV scans performed in 0.5 M H_2SO_4 from -0.2 V to 1.2 V (vs Ag/AgCl) at scan rates of 10, 25, 50, and 75 mV/s are shown in **Figure 8c**, with the 10 mV/s scan shown separately in **Figure 8d**. The CV scans indicate hydrogen adsorption and desorption at potentials less than 0 V, as well as characteristic oxidation and reduction peaks for palladium greater than 0.5 V.

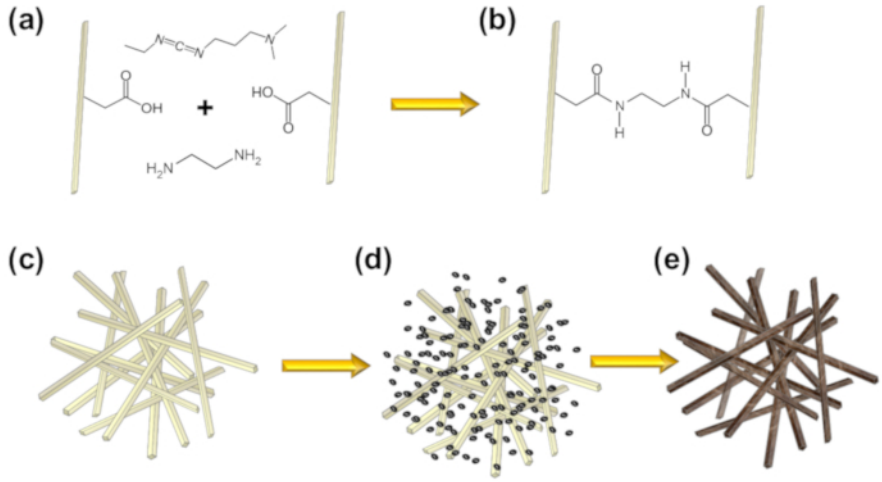

Figure 1. Aerogel synthesis scheme. (**a**) Cross linking carboxymethyl cellulose nanofibers (CNF) with EDC and ethylenediamine as a linker molecule. (**b**, **c**) Cross-linked carboxymethyl cellulose nanofibers. (**d**) CNF hydrogel equilibrated with palladium salt solution. (**e**) CNF biotemplated palladium composite aerogel after reduction with $NaBH_4$, rinsing, solvent exchange with ethanol, and CO_2 supercritical drying. Reproduced from reference 26 with permission. Please click here to view a larger version of this figure.

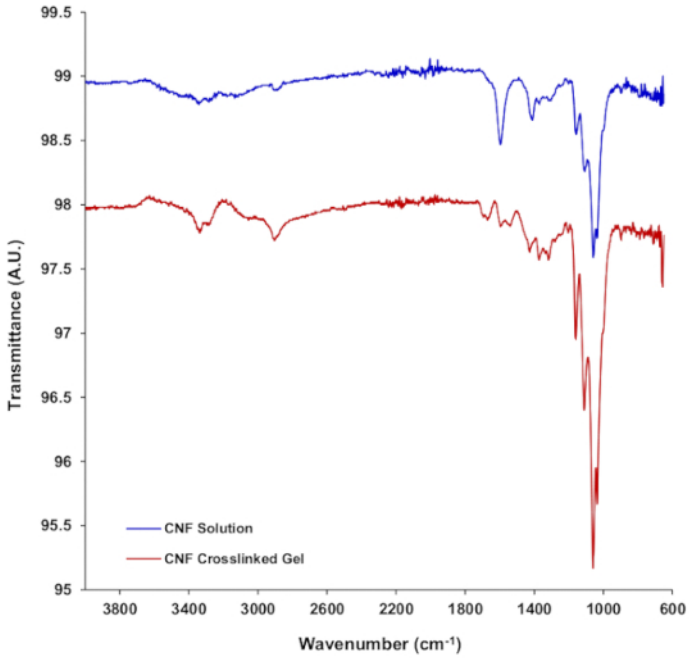

Figure 2. FTIR spectra for 3% (w/w) carboxymethyl cellulose nanofiber (CNF) solution in deionized water and CNF hydrogels crosslinked with 1-ethyl-3-(3-dimethylaminopropyl) carbodiimide hydrochloride (EDC) in the presence of ethylenediamine and subsequently equilibrated in deionized water. Please click here to view a larger version of this figure.

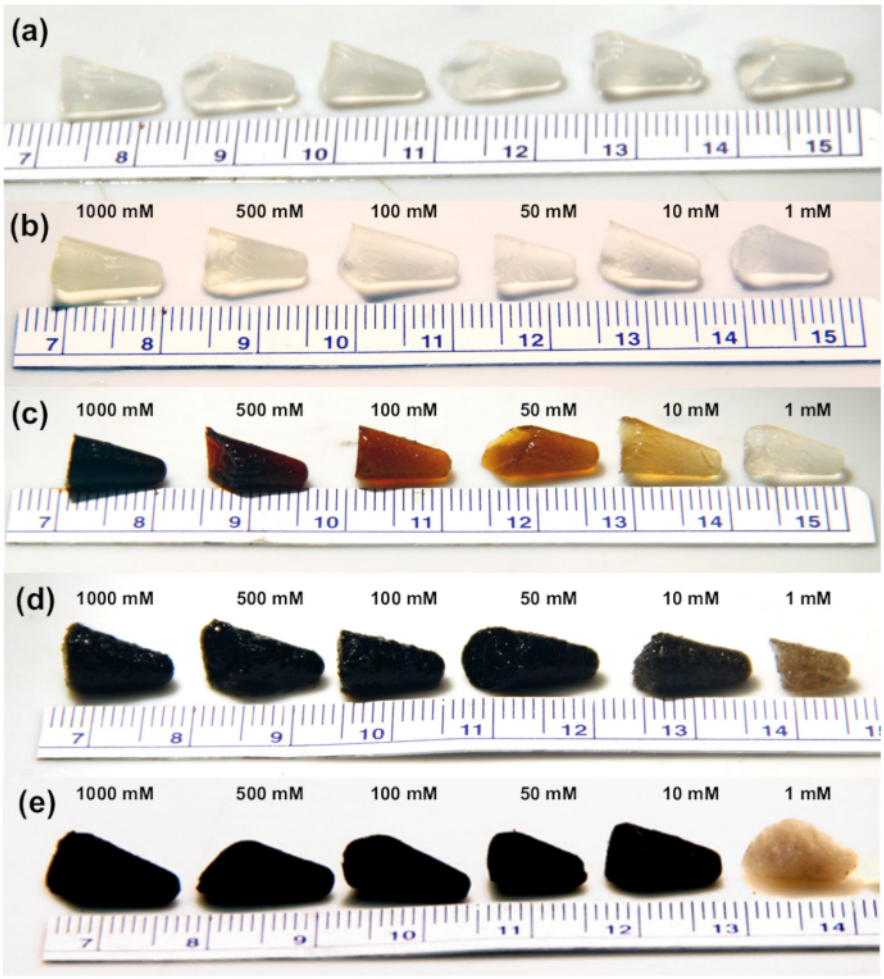

Figure 3. Aerogel synthesis process photos. (**a**) Cross-linked carboxymethyl cellulose nanofiber hydrogels with EDC and ethylenediamine as a linker molecule. CNF hydrogels equilibrated with palladium salt solutions of 1, 10, 50, 100, 500, and 1000 mM for (**b**) $Pd(NH_3)_4Cl_2$, and (**c**) Na_2PdCl_4. (**d**) CNF biotemplated palladium aerogel after reduction with $NaBH_4$. (**e**) CNF-Pd composite aerogels after rinsing, solvent exchange with ethanol, and CO_2 supercritical drying. Reproduced from reference 26 with permission. Please click here to view a larger version of this figure.

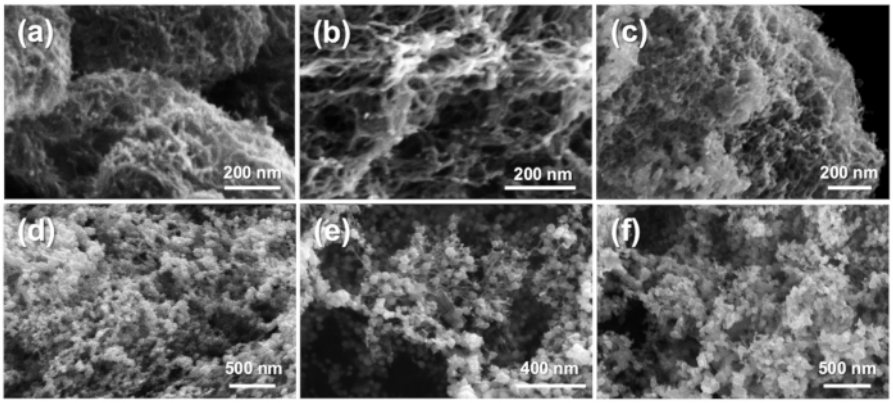

Figure 4. Scanning electron microscopy images of CNF-Pd composite aerogels prepared from $Pd(NH_3)_4Cl_2$ concentrations of (a) 1 mM; (b) 10 mM; (c) 50 mM; (d) 100 mM; (e) 500 mM; and (f) 1000 mM. Reproduced from reference 26 with permission. Please click here to view a larger version of this figure.

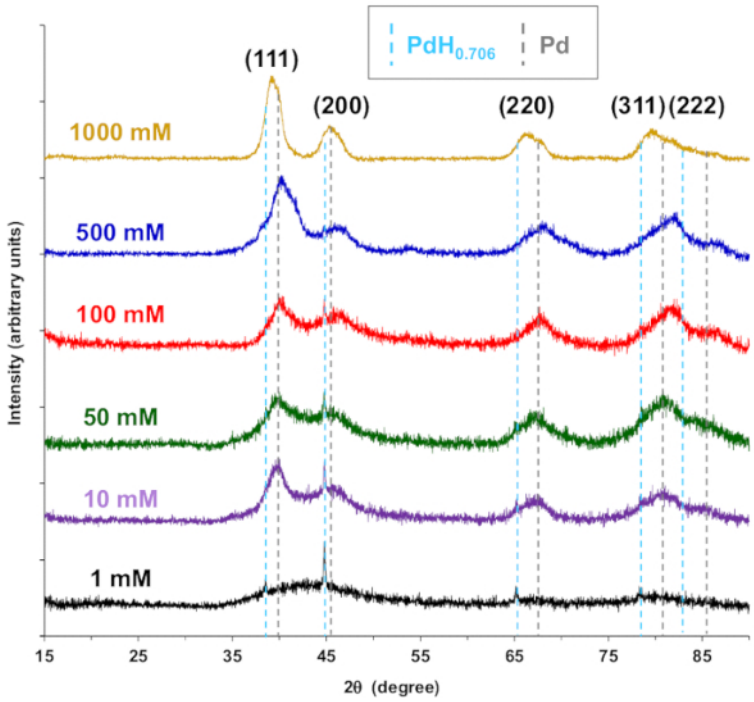

Figure 5. X-ray diffraction spectra for CNF-Pd composite aerogels synthesized from $Pd(NH_3)_4Cl_2$ salt solution concentrations of 1 mM, 10 mM, 50 mM, 100 mM, 500 mM, and 1000 mM. JCPDS reference 00-018-0951 palladium hydride peak positions are indicated with a light blue dashed line, and dashed gray lines for 01-087-0643 palladium peak positions. Reproduced from reference 26 with permission. Please click here to view a larger version of this figure.

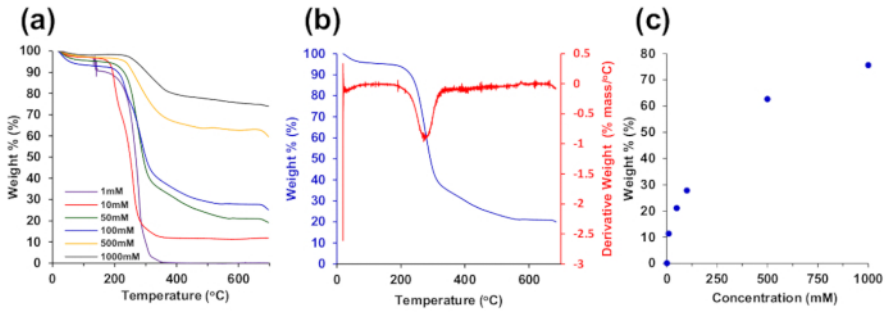

Figure 6. Thermogravimetric analysis (TGA). (**a**) TGA of aerogels synthesized with $Pd(NH_3)_4Cl_2$ salt solutions. (**b**) TGA of 50 mM $Pd(NH_3)_4Cl_2$ sample from (**a**) with differential thermal analysis (DTA). (**c**) Palladium sample mass at 600 °C from (**a**) for the varying palladium concentrations. Reproduced from reference 26 with permission. Please click here to view a larger version of this figure.

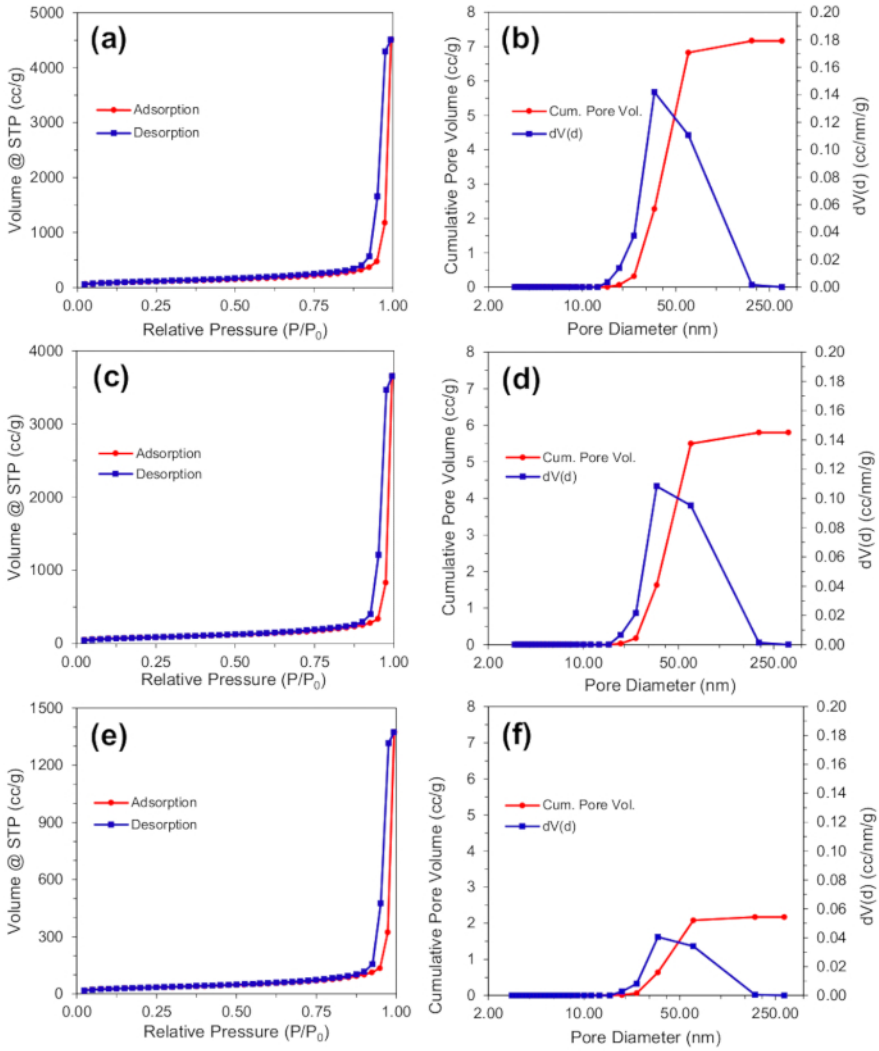

Figure 7. Brunauer-Emmett-Teller analysis. Nitrogen adsorption-desorption isotherms, and pore size distribution with cumulative pore volume for aerogels synthesized with $Pd(NH_3)_4Cl_2$ salt solutions of (**a,b**) 0 mM, (**c,d**) 100 mM and (**e,f**) 1000 mM. Reproduced from reference 26 with permission. Please click here to view a larger version of this figure.

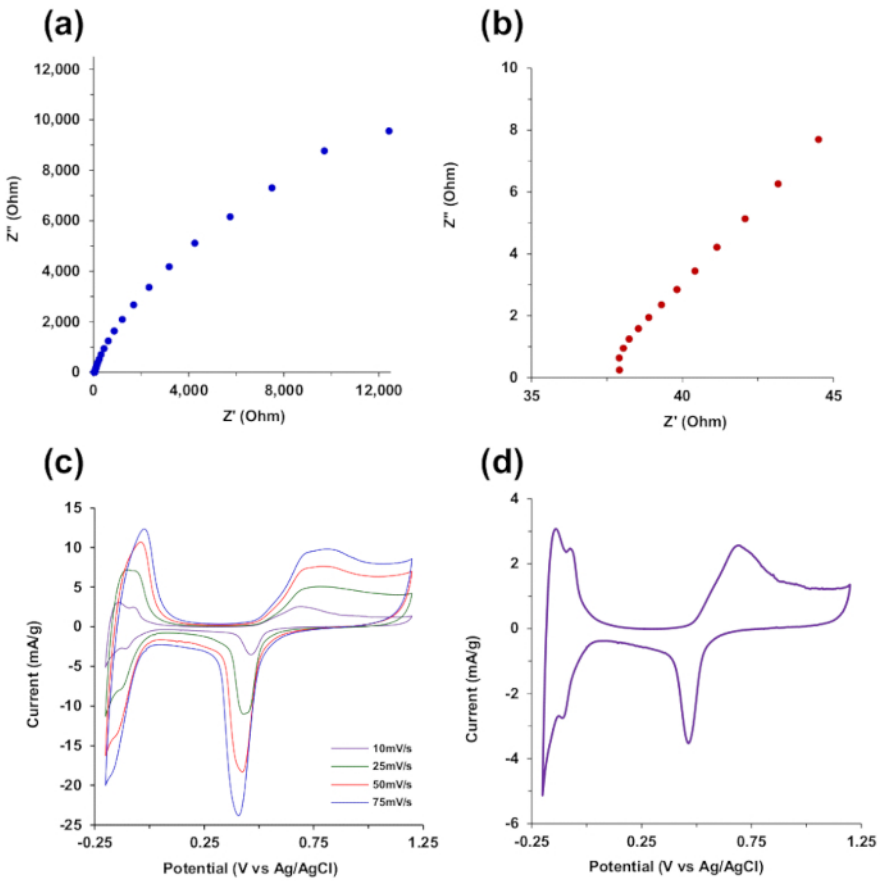

Figure 8. Electrochemical characterization in 0.5 M H_2SO_4 of CNF-Pd aerogels prepared from 1000 mM $Pd(NH_3)_4Cl_2$. (**a**) Electrochemical impedance spectroscopy with a 10 mV sine wave was used across frequencies from 140 kHz to 15 mHz. (**b**) High frequency spectra from 140 kHz to 1.3 kHz from (**a**). (**c**) Cyclic voltammetry (CV) at scan rates of 10, 25, 50, and 75 mV/s. (**d**) CV scan at 10 mV/s from (**c**). Reproduced from reference 26 with permission. Please click here to view a larger version of this figure.

Discussion

The noble metal cellulose nanofiber biotemplated aerogel synthesis method presented here results in stable aerogel composites with tunable metal composition. The covalent crosslinking of the compacted cellulose nanofibers after centrifugation results in hydrogels that are mechanically durable during the subsequent synthesis steps of palladium ion equilibration, electrochemical reduction, rinsing, solvent exchange, and supercritical drying. The hydrogel stability is vital during the electrochemical reduction step given the high concentration (2 M $NaBH_4$) of reducing agent solution and consequent violent hydrogen evolution. The commercially purchased TEMPO-oxidized cellulose nanofibrils used in this study had a nominal $-COO^-Na^+$ density of 1.2 mmol/g with approximate length and width of the cellulose nanofibers of 300 and 10 nm, respectively, and the 3% (w/w) solutions had a pH of 5. Likely due to the short fiber length, crosslinking at concentrations 3% (w/w) and less did not result in stable hydrogels. Centrifuging the 3% (w/w) solutions to compact the fibers to an approximate concentration of 3.8% (w/w) resulting in well crosslinked hydrogels that were stable during the electrochemical reduction of palladium step. The high $NaBH_4$ concentration is necessary to drive the reducing agent diffusion into the hydrogel biotemplate. The preservation of the covalent hydrogel macroscopic shape and biotemplated mesoporous structure is a key advantage of this synthesis method. In the absence of covalent crosslinking using EDC in the presence of a diamine linker, compacted ionic CNF hydrogels disaggregate during the chemical reduction step. Further, no palladium nanoparticles were observed to diffuse away from the CNF-palladium aerogel composites during the reduction step suggesting that all of the reduced palladium is bound within the resulting aerogels.

Critical to synthesizing homogenous aerogel composites is to allow sufficient time for diffusion in each of the synthesis steps. Using shorter times than indicated in the protocol will result in unstable gels and incomplete metallization throughout the cross-section of the aerogels. This manifests in disaggregation during the reduction, rinsing, solvent exchange, and drying steps, and a ring-like metallization pattern in the aerogel cross-section with metallization near the outer surface and incomplete metallization, or bare cellulose toward the center of the monolith.

The presented synthesis method's primary benefit is the ability to control the aerogel monolith shape, control the composite aerogel metal content, and achieve a high surface area mesoporous structure. Material characterization with SEM, XRD, TGA, nitrogen gas adsorption, EIS, and CV indicate meaningful and reproducible results that correlate well with the nanostructures observed with SEM.Further, other noble metal salts such as $HAuCl_43H_2O$, K_2PtCl_4, $Pt(NH_3)_4Cl_2$, and Na_2PtCl_6 may be employed to achieve similar noble metal composite aerogels[11].

The protocol may be varied by changing the shape of the cellulose nanofiber covalent hydrogel template. Compacted CNFs may be shaped into flat films through spin coating, or conformally applied to arbitrary geometries and then crosslinked and processed in accordance with the

presented method. The primary limitation of the method is the dependence of each synthesis step on the diffusion time of chemical species correlating with the thickness of the biotemplate hydrogel, and consequent diffusion path length. This poses a practical limit on the size and thickness of the resulting aerogels. Future work includes mass transfer modeling to determine the practical limits of the synthesis method based on diffusion, as well as convective flow approaches to overcome these limitations. Another potential issue with extended use of the CNF-palladium aerogel composite for catalytic applications is palladium leaching with detachment of palladium nanoparticles from the CNF template.

The synthesis method presented here offers an advancement in mechanically stable, shape-controlled, high surface area composite noble metal aerogels with tunable metal content. The covalent cellulose nanofiber hydrogels provide a material synthesis approach for a range of metal composites for energy, catalysis, and sensor applications.

Disclosures

The authors have nothing to disclose.

Acknowledgements

The authors are grateful to Dr. Stephen Bartolucci and Dr. Joshua Maurer at the U.S. Army Benet Laboratories for the use of their scanning electron microscope. This work was supported by a Faculty Development Research Fund grant from the United States Military Academy, West Point.

References

1. Kistler, S. S. Coherent Expanded Aerogels and Jellies. *Nature.* **127** 741, (1931).
2. Du, A., Zhou, B., Zhang, Z., & Shen, J. A Special Material or a New State of Matter: A Review and Reconsideration of the Aerogel. *Materials.* **6** (3), 941, (2013).
3. Tappan, B. C., Steiner, S. A., & Luther, E. P. Nanoporous Metal Foams. *Angewandte Chemie International Edition.* **49** (27), 4544-4565, (2010).
4. Bigall, N. C. et al. Hydrogels and Aerogels from Noble Metal Nanoparticles. *Angewandte Chemie International Edition.* **48** (51), 9731-9734, (2009).
5. Ranmohotti, K. G. S., Gao, X., & Arachchige, I. U. Salt-Mediated Self-Assembly of Metal Nanoshells into Monolithic Aerogel Frameworks. *Chemistry of Materials.* **25** (17), 3528-3534, (2013).
6. Gao, X., Esteves, R. J., Luong, T. T. H., Jaini, R., & Arachchige, I. U. Oxidation-Induced Self-Assembly of Ag Nanoshells into Transparent and Opaque Ag Hydrogels and Aerogels. *Journal of the American Chemical Society.* **136** (22), 7993-8002, (2014).
7. Herrmann, A.-K. et al. Multimetallic Aerogels by Template-Free Self-Assembly of Au, Ag, Pt, and Pd Nanoparticles. *Chemistry of Materials.* **26** (2), 1074-1083, (2014).
8. Ding, Y., Chen, M., & Erlebacher, J. Metallic Mesoporous Nanocomposites for Electrocatalysis. *Journal of the American Chemical Society.* **126** (22), 6876-6877, (2004).
9. Liu, W. et al. High-Performance Electrocatalysis on Palladium Aerogels. *Angewandte Chemie International Edition.* **51** (23), 5743-5747, (2012).
10. Shafaei Douk, A., Saravani, H., & Noroozifar, M. Three-dimensional assembly of building blocks for the fabrication of Pd aerogel as a high performance electrocatalyst toward ethanol oxidation. *Electrochimica Acta.* **275** 182-191, (2018).
11. Burpo, F. J. et al. Direct solution-based reduction synthesis of Au, Pd, and Pt aerogels. *Journal of Materials Research.* **32** (22), 4153-4165, (2017).
12. Burpo, F. J. et al. A Rapid Synthesis Method for Au, Pd, and Pt Aerogels Via Direct Solution-Based Reduction. *JoVE.* (136), e57875, (2018).
13. Qin, G. W. et al. A Facile and Template-Free Method to Prepare Mesoporous Gold Sponge and Its Pore Size Control. *The Journal of Physical Chemistry C.* **112** (28), 10352-10358, (2008).
14. Hench, L. L., & West, J. K. The Sol-Gel Process. *Chemical Reviews.* **90** (1), 33-72, (1990).
15. Sotiropoulou, S., Sierra-Sastre, Y., Mark, S. S., & Batt, C. A. Biotemplated Nanostructured Materials. *Chemistry of Materials.* **20** (3), 821-834, (2008).
16. Huang, J. et al. Bio-inspired synthesis of metal nanomaterials and applications. *Chemical Society Reviews.* **44** (17), 6330-6374, (2015).
17. Burpo, F. J., Mitropoulos, A. N., Nagelli, E. A., Ryu, M. Y., & Palmer, J. L. Gelatin biotemplated platinum aerogels. *MRS Advances.* 10.1557/adv.2018.489 1-6, (2018).
18. Jarvis, M. Cellulose stacks up. *Nature.* **426** 611, (2003).
19. Sirő, I. & Plackett, D. Microfibrillated cellulose and new nanocomposite materials: a review. *Cellulose.* **17** (3), 459-494, (2010).
20. Dufresne, A. Nanocellulose: a new ageless bionanomaterial. *Materials Today.* **16** (6), 220-227, (2013).
21. Grishkewich, N., Mohammed, N., Tang, J., & Tam, K. C. Recent advances in the application of cellulose nanocrystals. *Current Opinion in Colloid & Interface Science.* **29** 32-45, (2017).
22. Eyley, S., & Thielemans, W. Surface modification of cellulose nanocrystals. *Nanoscale.* **6** (14), 7764-7779, (2014).
23. Missoum, K., Belgacem, M., & Bras, J. Nanofibrillated Cellulose Surface Modification: A Review. *Materials.* **6** (5), 1745, (2013).
24. Li, Z., Yao, C., Wang, F., Cai, Z., & Wang, X. Cellulose nanofiber-templated three-dimension TiO_2 hierarchical nanowire network for photoelectrochemical photoanode. *Nanotechnology.* **25** (50), 504005, (2014).
25. Koga, H. et al. Uniformly connected conductive networks on cellulose nanofiber paper for transparent paper electronics. *Npg Asia Materials.* **6** e93, (2014).
26. Burpo, F. et al. Cellulose Nanofiber Biotemplated Palladium Composite Aerogels. *Molecules.* **23** (6), 1405, (2018).
27. Gu, J., Hu, C., Zhang, W., & Dichiara, A. B. Reagentless preparation of shape memory cellulose nanofibril aerogels decorated with Pd nanoparticles and their application in dye discoloration. *Applied Catalysis B: Environmental.* **237** 482-490, (2018).

28. Coates, J. in *A Practical Approach. In Encyclopedia of Analytical Chemistry* .doi:10.1002/9780470027318.a5606 (ed R. A. Meyers and M. L. McKelv) (2006).
29. Wang, S. et al. Cellulose nanofiber-assisted dispersion of cellulose nanocrystals@polyaniline in water and its conductive films. *RSC Advances.* **6** (12), 10168-10174, (2016).
30. Grabarek, Z., & Gergely, J. Zero-length crosslinking procedure with the use of active esters. *Analytical Biochemistry.* **185** (1), 131-135, (1990).
31. Shabanpour, B., Kazemi, M., Ojagh, S. M., & Pourashouri, P. Bacterial cellulose nanofibers as reinforce in edible fish myofibrillar protein nanocomposite films. *International Journal of Biological Macromolecules.* **117** 742-751, (2018).
32. Brunauer, B., Emmett, P., & Teller, P. Adsorption of gases in multimolecular layers. *Journal of the American Chemical Society.* **60**, (1938).
33. Barrett, E., Joyner, L., & Halenda, P. The determination of pore volume and area distributions in porous substances. I. Computations from nitrogen isotherms. *Journal of the American Chemical Society.* **73**, (1951).

